Mathematical Biosciences and Engineering

MBE, 20(11): 19454–19467.
DOI: 10.3934/mbe.2023861
Received: 07 March 2023
Revised: 02 September 2023
Accepted: 18 September 2023
Published: 20 October 2023

http://www.aimspress.com/journal/MBE

Research article

Colon histology slide classification with deep-learning framework using individual and fused features

Venkatesan Rajinikanth[1], Seifedine Kadry[2,3,4], Ramya Mohan[1], Arunmozhi Rama[1], Muhammad Attique Khan[5] and Jungeun Kim[6,*]

[1] Department of Computer Science and Engineering, Division of Research and Innovation, Saveetha School of Engineering, SIMATS, Chennai 602105, India
[2] Department of Applied Data Science, Noroff University College, 4612 Kristiansand, Norway
[3] Artificial Intelligence Research Center (AIRC), College of Engineering and Information Technology, Ajman University, Ajman 346, United Arab Emirates.
[4] Department of Electrical and Computer Engineering, Lebanese American University, Byblos 1401, Lebanon.
[5] Department of Computer Science and Mathematics, Lebanese American University, Beirut, Lebanon
[6] Department of Software, Kongju National University, Cheonan, 31080, Korea

* **Correspondence:** Email: jekim@kongju.ac.kr.

Abstract: Cancer occurrence rates are gradually rising in the population, which reasons a heavy diagnostic burden globally. The rate of colorectal (bowel) cancer (CC) is gradually rising, and is currently listed as the third most common cancer globally. Therefore, early screening and treatments with a recommended clinical protocol are necessary to trat cancer. The proposed research aim of this paper to develop a Deep-Learning Framework (DLF) to classify the colon histology slides into normal/cancer classes using deep-learning-based features. The stages of the framework include the following: (i) Image collection, resizing, and pre-processing; (ii) Deep-Features (DF) extraction with a chosen scheme; (iii) Binary classification with a 5-fold cross-validation; and (iv) Verification of the clinical significance. This work classifies the considered image database using the follwing: (i) Individual DF, (ii) Fused DF, and (iii) Ensemble DF. The achieved results are separately verified using binary classifiers. The proposed work considered 4000 (2000 normal and 2000 cancer) histology slides for the examination. The result of this research confirms that the fused DF helps to achieve a detection accuracy of 99% with the K-Nearest Neighbor (KNN) classifier. In contrast, the individual and ensemble DF provide classification accuracies of 93.25 and 97.25%, respectively.

Keywords: colorectal cancer; histology slide; fused features; ensemble features; classification

1. Introduction

A number of research works have been conducted throughout the world in order to develop more advanced medical diagnostic facilities to support the accurate detection of diseases so that an effective treatment can be executed. Once the diagnostic scheme is developed, it can be tested and recommended for practical use. Despite the fact that there are a number of modern facilities available, their accessibility is limited due to various economic factors. The available diagnostic facilities in high-income and upper-middle-income countries are comparatively more advanced than those available in lower-middle and low-income countries [1,2]. In order to support early and precise disease detection procedures, several research projects are currently being conducted in an effort to develop an appropriate scheme to support this process.

It has been shown in a recent publication that, regardless of the economic condition of a country, the incidence rate of acute and infectious diseases among humans is on the rise worldwide due to a number of factors, including the following: (i) heredity, (ii) immunodeficiency, (iii) age, and (iv) environmental factors [3,4]. It has been observed that the rapid increase in disease occurrence rates in humans causes various medical burdens, from diagnosis to treatment; this burden has an adverse effect on the economy and the health system of the country.

According to the annual report of the World Health Organisation (WHO) for 2020, the incidence rate of cancer is gradually increasing throughout the world and early detection and treatment of cancer are of the utmost importance when it comes to preventing mortality as a result of the disease. According to the report, breast, lung, and colorectal cancer (CC) have higher incident rates when compared to other types of cancers [5]. There are 1.9 million new cases of CC every year, making it the third most common cancer worldwide. It is possible to access a detailed report about CC by visiting [6].

CC occurs when cells within the colon/rectum grow out of control. Polyps begin as the first stage, and if left untreated, polyps may develop into cancer. In order to reduce the risk rate, early screening and treatment are essential. There are several commonly performed clinically level screening procedures that can be used to assess and test for CC and its severity, such as personal examinations by doctors, colonoscopy/endoscopy-supported assessments and a biopsy collection for microscopic image examinations. Amongst these, the microscopy images play a vital role in detecting the harshness and the stage of the CC, which is essential to plan the appropriate treatment, such as radiation therapy, chemotherapy and surgery [7,8]. Most of the current clinical procedures use the whole slide images (WSI) collected using a prescribed protocol to implement an inspection by the disease expert. To reduce the diagnostic burden, computerized procedures are implemented in clinics to support a faster and timely detection of CC from histology slides. Examination of the WSI using the computer algorithm requires a few chosen image pre-processing techniques; patch based analysis is one of the common procedures in which the WSI is cropped and resized into several small sections [9]. Then these images are examined using the chosen computerized approaches.

To detect CC using the chosen biomedical imaging technique, numerous frameworks have been proposed and implemented in the literature for the detection of the disease. This work is aimed at developing and implementing a deep-learning framework (DLF), which will be used to detect CC on histological slides by using deep-learning. As part of the proposed DLF, there are a number of phases,

including the following: (i) the collection, resizing, and preprocessing of histology slides; (ii) deep-features mining using the preferred method; (iii) binary categorization with a fivefold cross-validation; and (iv) verifying the clinical significance of the developed system using a benchmark histology slide database. For the CC histology slide data set, the proposed work seeks to test the performance of pre-trained deep learning schemes with the following features, using binary classifiers chosen from a variety of sources: (i) individual features, (ii) fused dual deep features, and (iii) an ensemble of features. As part of the evaluation and verification of the detection performance CC, SoftMax, Naive Bayes (NB), Decision Trees (DT), K-Nearest Neighbor (KNN) and Support Vector Machines (SVM) are separately evaluated and verified. The experimental results of this study confirms that the fused deep-feature (VGG16 + ResNet101) provides a CC detection accuracy of 99% with the KNN classifier.

As a result of this research, the main contribution of this paper is the evaluation of the performance of commonly available pre-trained models applying individual, merged, and ensemble features on a chosen histopathology image database of the CC, all with quite promising results. Furthermore the clinical significance is verified using the benchmark WSI of the Gland Segmentation (GlaS) dataset [10,11].

The remaining sections of this work are arranged as follows: Section 2 presents the literature review, Section 3 discusses the methodology and Sections 4 and 5 demonstrate the experimental outcome and results of this study, respectively.

2. Literature review

Table 1. Summary of medical data based cancer detection schemes.

Reference	Methodology	Outcome (Accuracy %)
Bukhari et al. [12]	Self-supervised learning supported diagnosis of the colon histology slide is examined and the ResNet50 scheme provided an approved classification result.	93.91
Mangal et al. [13]	Examination of colon and lung histology slide is demonstrated using a convolutional neural network (CNN).	96.61
Masud et al. [14]	Machine and deep-learning associated framework is proposed to analyze the colon and lung histology slides.	96.33
Ali and Ali [15]	Cancer detection in colon and lung histology slides are discussed using multi-input dual-stream capsule network	99.58
Sarwinda et al. [16]	ResNet18 and ResNet50 supported scheme to detect the cancer in colon histology image is discussed.	>80
Hamida et al. [17]	Deep-learning supported detection of CC in histology image is presented.	>98.66
Ohata et al. [18]	Transfer-learning supported classification of histological images to detect the CC is presented.	92.083
Fan et al. [19]	Transfer-learning supported CC detection from colon histology slide is presented.	99.29

Due to a steady increase in cancer occurrence rates, scientists and researchers have undertaken several research projects to support the automatic and precise detection of cancer based on available medical data. The purpose of this section is to summarize the selected recent CC detection works that have used the medical image-based scheme as a means to detect the occurrence of CCs and their severity, as shown in Table 1.

Table 1 presents the earlier works executed to examine CC using a chosen computerized technique. Most of these works were implemented using the available histology slides of a chosen image database. These existing works were not tested on the WSI, and hence, the proposed research aims to develop and implement an appropriate CC detection procedure which works well on the chosen histology datasets.

3. Methodology

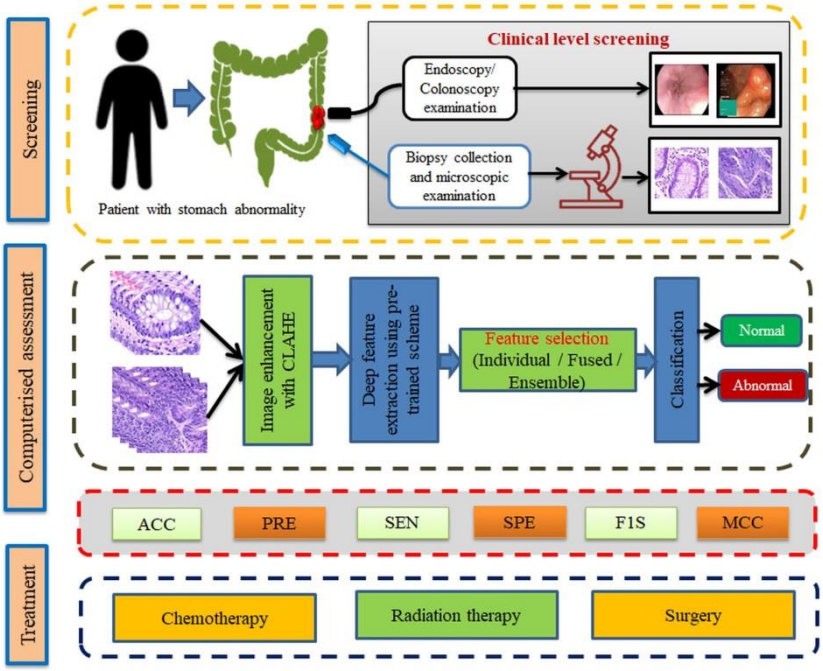

Figure 1. Proposed CC detection framework.

This part of the research presents the DLF developed to detect the CC using histology slides. The complete information is presented in Figure 1. The screening stage is performed in hospitals when patients visit with CC symptoms. The standard tests involve; a physical check by a doctor, an endoscopy/colonoscopy examination, and biopsy collection and analysis. The treatment procedure for CC mainly depends on the cancer stage, and can be detected by biopsy with the chosen microscopic examination. Therefore, an assessment of the histology slide is essential in CC diagnosis, and this work proposes a DLF for a computerized assessment. This research considers the histology slides of CC for the examination and computerized examination section. Figure 1 confirms that the proposed technique follows a straightforward methodology, from feature extraction to classification. This work implements a 50% dropout in the extracted DLF to avoid the overfitting issue. The various stages of this scheme are as follows; image enhancement with Contrast-Limited Adaptive

Histogram Equalization (CLAHE) [20,21], deep-feature extraction, feature vector generation based on the need (individual/fused/ensemble), and classification. In this work, a five-fold cross-validation is employed, and the best result is considered to validate the performance of the developed system. This scheme helps the doctor obtain the initial examination of CC, and the treatment must be planned and implemented by the doctor based on the severity of the CC.

3.1 Image database

This research considered the histological test images found in the LC25000 dataset [22] for the initial training and verification of the proposed scheme and the GlaS dataset [10,11] for confirming the clinical significance. The initial database consists of 10,000 images (5000 normal and 5000 cancerous images) of the CC and to verify the performance of the pre = trained models, only 40% (4000) images are considered. The sample test images considered in this study are presented in Figure 2, and the number of images considered is depicted in Table 2. The sample GlaS image is presented in Figure 3, in which Figure 3(a) depicts the benign class and Figure 3(b) presents the malignant class. From each image, 4×4 (16) slices are cropped and resized to $224\times224\times3$ pixels to obtain a validation image dimension of 400 (200 benign and 200 malignant). The outcome of the proposed DLF confirms that the developed scheme works well on the considered image databases.

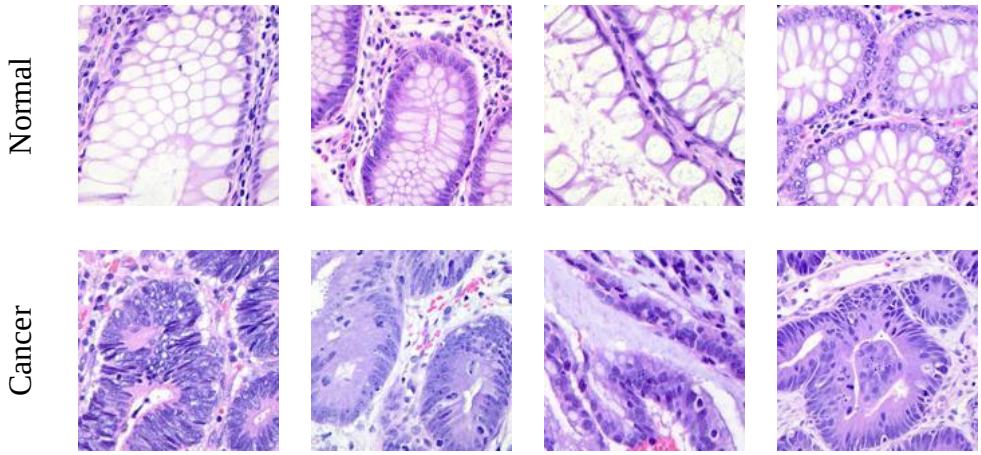

Figure 2. Sample test images of LS25000.

Table 2. Images considered in verifying the performance of developed scheme.

Class	Dimension	Images considered			
		Total	Training	Testing	Validation
Normal	$224\times224\times3$	2000	1600	200	200
Cancer	$224\times224\times3$	2000	1600	200	200

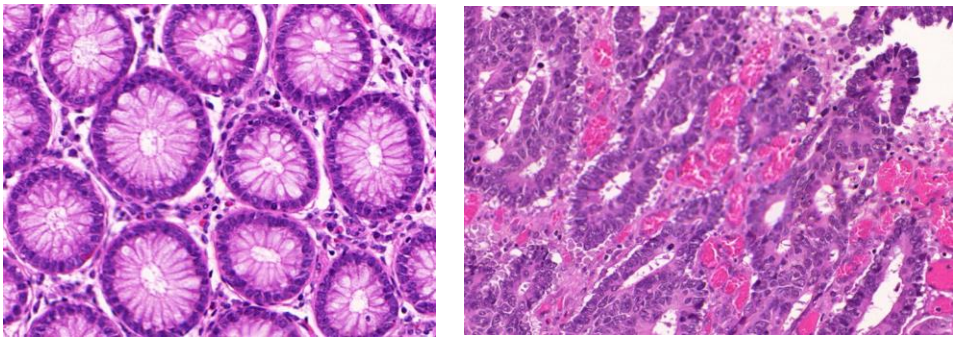

(a) Benign (b) Malignant

Figure 3. Sample test images from GlaS.

3.2 Deep-learning scheme

Due to its merit and clinical significance, pre-trained and customary deep-learning-based methods are widely employed to examine the medical database. Compared to the customized DLF, the pre-trained models are easily accessible and implementable. Hence, these methods are widely employed in the literature to examine the biomedical images of a chosen modality. This work considered pre-trained schemes, such as VGG16, VGG19, ResNet18, ResNet34, ResNet50, ResNet101, and DenseNet201, for the examination [23–25]. Initially, the conventional image augmentation procedure (horizontal/vertical flip, rotation with an angle of 30 º, zoom range of 0.3, and width/height shift with a range of 0.3) is employed to increase the number of images to improve the performance of the training process. Furthermore, the following initial values are assigned for the considered deep-learning system to support an improved diagnosis on the chosen database: initialweights = ImageNet, batch value = 8, epochs = 150, optimizer = Adam, pooling = max, supervise metric = accuracy, and loss, classifier = SoftMax with 5-fold cross-validation [26,27].

3.3 Implementation

The, the considered scheme is implemented using individual features with a dimension of $1\times1\times1000$, fused features with a dimension of $1\times1\times1000$ and ensemble features with a dimension of $1\times1\times1000$. During the individual features based assessment, the deep-features obtained (Eq (1)) from DLF is considered to verify the performance of the binary classifiers. During the fused features approach, the top two DLF features (VGG16 and resNet101) are considered, and these features are sorted based on its rank before applying a 50% dropout to obtain a reduced features vector of dimension $1\times1\times500$. The fused feature vector is achieved by serially combining these two features in order to obtain a single feature vector with a dimension of $1\times1\times1000$, as presented in Eq (2). During the ensemble feature selection process, the average feature among VGG16, VGG19, ResNet101 and DenseNet201 are considered to form a new feature vector with the dimension $1\times1\times1000$, as shown in Eq (3).

$$Individual_{(1\times1\times1000)} = DF_{(1\times1\times1)}, DF_{(1\times1\times2)}, \ldots, DF_{(1\times1\times1000)} \tag{1}$$

$$Fused_{(1\times1\times1000)} = DF1_{(1\times1\times500)} + DF2_{(1\times1\times500)} \tag{2}$$

$$Ensemble_{(1\times1\times1000)} = [DF1_{(1\times1\times1000)} + DF2_{(1\times1\times1000)} + DF3_{(1\times1\times1000)} + DF4_{(1\times1\times1000)}] \div 4 \tag{3}$$

Then, the classification task is separately implemented with these features, and the achieved results for the chosen classifiers are individually presented and discussed.

3.4 Performance evaluation and validation

The CC detection performance of the proposed DLF is verified using a binary classification scheme with different feature vector. During this process, the necessary values such as true-positive (TP), true-negative (TN), false-positive (FP), and false-negative (FN) are computed. From these values, other essential measures such as accuracy (ACC), precision (PRE), sensitivity (SEN), specificity (SPE), F1 Score (F1S), are Matthew's Correlation Coefficient (MCC) are computed, and the mathematical notation for these values are depicted in Eqs (4)–(9). In this work, the binary classifiers, such as SoftMax, NB, DT, KNN and SVM, are considered, and the necessary information regarding these classifiers are available in [28–30].

$$ACC = \frac{TP + TN}{TP + TN + FP + FN} \tag{4}$$

$$PRE = \frac{TP}{TP + FP} \tag{5}$$

$$SEN = \frac{TP}{TP + FN} \tag{6}$$

$$SPE = \frac{TN}{TN + FP} \tag{7}$$

$$F1S = \frac{2TP}{2TP + FN + FP} \tag{8}$$

$$MCC = \frac{(TP \times TN) - (FP \times FN)}{\sqrt{(TP + FP)(TP + FN)(TN + FP)9TN + FN)}} \tag{9}$$

4. Results and discussion

This section demonstrates the experimental outcome and its discussions. The implemented research was performed using a workstation containing an Intel i5 processor, 16GB RAM and 4GB VRAM operational with Python®. This work was initially implemented on the LS25000 dataset and then the GlaS dataset and the results are discussed.

The proposed investigation was initially performed using the deep individual features and SoftMax classifier. The achieved result for various DLFs for the five-fold cross-validation is presented in Table 3. This table confirms that the VGG16 helps in obtaining an improved accuracy compared to other methods. ResNet101 is ranked second based on overall performance and DenseNet201 is ranked third. Table 4 presents the outcome of the 5-fold cross-validation and the selected best outcome with the VGG16. Figure 4 presents the results achieved from various layers of VGG16, in which Figure 4(a) presents the sample image and Figure 4(b)–(f) denotes the various layer outcomes.

After analyzing the performance of the proposed scheme with a unique feature, the classification task is repeated using fused features and the ensemble of deep features, as discussed in Eqs (2) and (3), and the achieved results are presented.

Figure 5 presents the confusion matrix (CM) achieved with this study, in which Figure 5(a) presents the CM for fused features and Figure 5(b) presents the CM for ensemble features. The TP, TN, FP, and FN present in these CM, confirm that these schemes help to achieve a better accuracy. Figure 6 depicts the results achieved when the ensemble of features is used. Figure 6(a),(b) shows the accuracy and loss for the training and validation process and Figure 6(c) presents the receiver operating characteristic (ROC) curve having a value of no skill area under curve (AUC) of 0.50 and a logistic AUC of 0.98, which confirms the significance of the implemented scheme. Similar results are computed for all other procedures considered in this study, and the results are demonstrated.

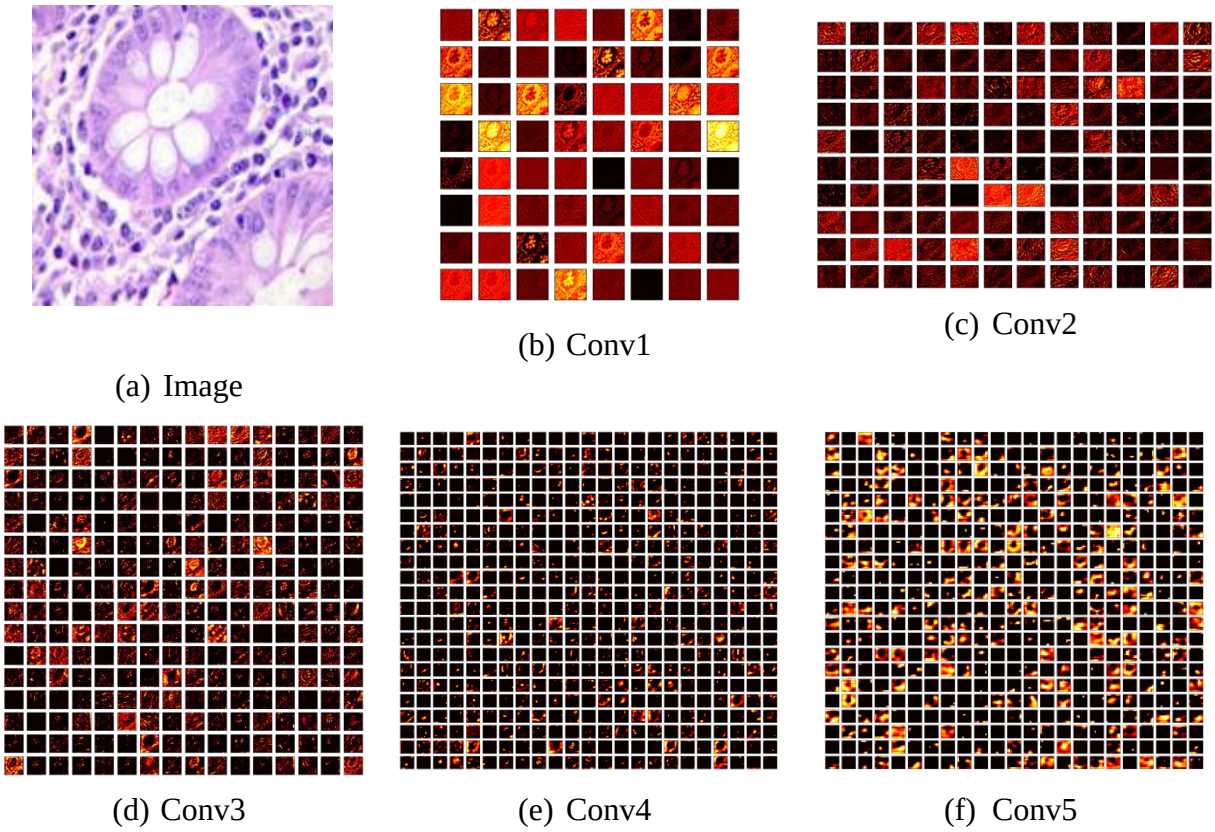

(a) Image (b) Conv1 (c) Conv2

(d) Conv3 (e) Conv4 (f) Conv5

Figure 4. Convolutional layer results from VGG16.

Table 3. Experimental outcome of pre-trained models with SoftMax classifier.

Scheme	TP	FN	TN	FP	ACC	PRE	SEN	SPE	F1S	MCC
VGG16	184	17	188	11	93.0000	94.3590	91.5423	94.4724	92.9293	86.0405
VGG19	185	13	186	16	92.7500	92.0398	93.4343	92.0792	92.7318	85.5103
ResNet18	181	23	181	15	90.5000	92.3469	88.7255	92.3469	90.5000	81.0724
ResNet34	183	16	186	15	92.2500	92.4242	91.9598	92.5373	92.1914	84.5003
ResNet50	184	17	186	13	92.5000	93.4010	91.5423	93.4673	92.4623	85.0181
ResNet101	187	12	186	15	93.2500	92.5743	93.9698	92.5373	93.2668	86.5104
DenseNet201	186	12	185	17	92.7500	91.6256	93.9394	91.5842	92.7681	85.5289

Table 4. VGG16 result for five-fold cross validation.

Scheme	TP	FN	TN	FP	ACC	PRE	SEN	SPE	F1S	MCC
Fold1	181	17	184	18	91.2500	90.9548	91.4141	91.0891	91.1839	82.5002
Fold2	183	19	184	14	91.7500	92.8934	90.5941	92.9293	91.7293	83.5286
Fold3	183	12	186	18	92.4812	91.0448	93.8462	91.1765	92.4242	85.0034
Fold4	184	17	188	11	93.0000	94.3590	91.5423	94.4724	92.9293	86.0405
Fold5	182	16	184	16	91.9598	91.9192	91.9192	92.0000	91.9192	83.9192

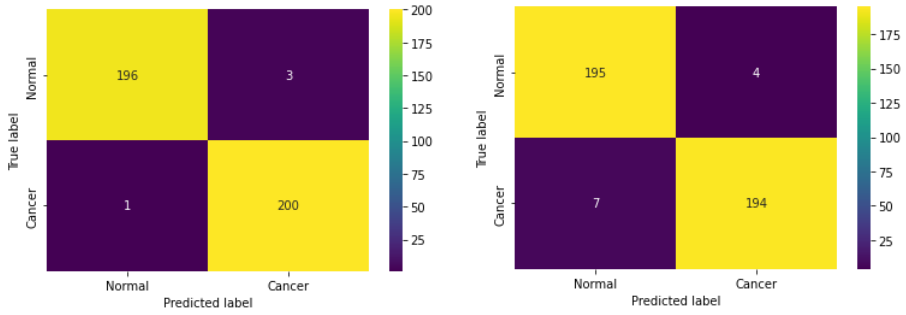

(a) Fused (b) Ensemble

Figure 5. Confusion matrix achieved for various feature set.

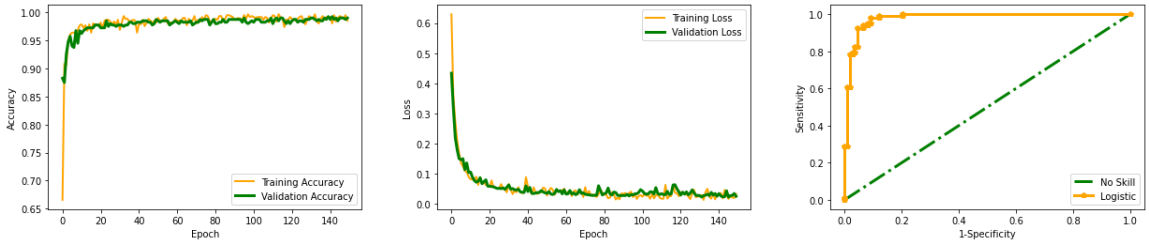

(a) Accuracy (b) Loss (c) RoC

Figure 6. Search convergence and the AUC curve.

Table 5 presents the experimental outcome achieved in this study with individual features (VGG16 and ResNet101), fused features, and ensemble features. The binary classification with a 5-fold cross-validation helps to achieve an improved classification accuracy from 93% (VGG16 with SoftMax) to 99% (fused features with KNN). This confirms that the proposed DLF works well on the LS25000 database. To verify the clinical significance of the proposed technique, the WSI of the GlaS database is also considered, and the achieved result is depicted in Table 6. This table confirms that the classification achieved good results (benign/malignant class) with both the fused and ensemble features. With the fused features, the DT classifier provided an accuracy of 97.25%, and with the ensemble features, the NB classifier achieved an accuracy of 97%. The Glyph-Plot shown in Figure 7 depicts the overall performance achieved with the proposed DLF. This confirms that the proposed scheme works well on the histology images; in the future, it can be considered to examine the clinically collected histology images of CC cancer.

Table 5. Experimental results with different feature set.

Scheme		TP	FN	TN	FP	ACC	PRE	SEN	SPE	F1S	MCC
VGG16	SoftMax	**184**	**17**	**188**	**11**	**93.0000**	**94.3590**	**91.5423**	**94.4724**	**92.9293**	**86.0405**
	NB	183	14	188	15	92.7500	92.4242	92.8934	92.6108	92.6582	85.4989
	DT	184	16	187	13	92.7500	93.4010	92.0000	93.5000	92.6952	85.5096
	KNN	188	14	183	15	92.7500	92.6108	93.0693	92.4242	92.8395	85.4989
	SVM	187	14	185	14	93.0000	93.0348	93.0348	92.9648	93.0348	85.9996
ResNet101	SoftMax	**187**	**12**	**186**	**15**	**93.2500**	**92.5743**	**93.9698**	**92.5373**	**93.2668**	**86.5104**
	NB	185	16	187	12	93.0000	93.9086	92.0398	93.9698	92.9648	86.0183
	DT	188	13	186	13	93.5000	93.5323	93.5323	93.4673	93.5323	86.9997
	KNN	186	15	186	13	93.0000	93.4673	92.5373	93.4673	93.0000	86.0047
	SVM	185	15	186	14	92.7500	92.9648	92.5000	93.0000	92.7318	85.5011
VGG16+ResNet101	SoftMax	197	2	196	5	98.2500	97.5248	98.9950	97.5124	98.2544	96.5110
	NB	198	3	194	5	98.0000	97.5369	98.5075	97.4874	98.0198	96.0045
	DT	197	2	197	4	98.5000	98.0100	98.9950	98.0100	98.5000	97.0049
	KNN	**200**	**1**	**196**	**3**	**99.0000**	**98.5222**	**99.5025**	**98.4925**	**99.0099**	**98.0048**
	SVM	196	3	197	4	98.2500	98.0000	98.4925	98.0100	98.2456	96.5012
Ensemble feature	SoftMax	192	8	193	7	96.2500	96.4824	96.0000	96.5000	96.2406	92.5012
	NB	194	5	191	10	96.2500	95.0980	97.4874	95.0249	96.2779	92.5297
	DT	193	6	194	7	96.7500	96.5000	96.9849	96.5174	96.7419	93.5012
	KNN	193	8	193	6	96.5000	96.9849	96.0199	96.9849	96.5000	93.0048
	SVM	**194**	**7**	**195**	**4**	**97.2500**	**97.9798**	**96.5174**	**97.9899**	**97.2431**	**94.5109**

Table 6. Experimental results with GlaS database.

Scheme		TP	FN	TN	FP	ACC	PRE	SEN	SPE	F1S	MCC
VGG16 + ResNet101	SoftMax	191	8	193	8	96.0000	95.9799	95.9799	96.0199	95.9799	91.9998
	NB	192	7	192	9	96.0000	95.5224	96.4824	95.5224	96.0000	92.0048
	DT	**195**	**5**	**194**	**6**	**97.2500**	**97.0149**	**97.5000**	**97.0000**	**97.2569**	**94.5012**
	KNN	194	7	194	5	97.0000	97.4874	96.5174	97.4874	97.0000	94.0049
	SVM	195	6	193	6	97.0000	97.0149	97.0149	96.9849	97.0149	93.9998
Ensemble feature	SoftMax	192	10	192	6	96.0000	96.9697	95.0495	96.9697	96.0000	92.0192
	NB	**193**	**6**	**195**	**6**	**97.0000**	**96.9849**	**96.9849**	**97.0149**	**96.9849**	**93.9998**
	DT	194	5	193	8	96.7500	96.0396	97.4874	96.0199	96.7581	93.5108
	KNN	192	7	194	7	96.5000	96.4824	96.4824	96.5174	96.4824	92.9998
	SVM	193	8	193	6	96.5000	96.9849	96.0199	96.9849	96.5000	93.0048

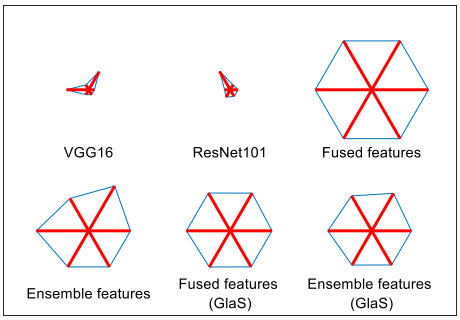

Figure 7. Glyph-Plot to present the overall performance.

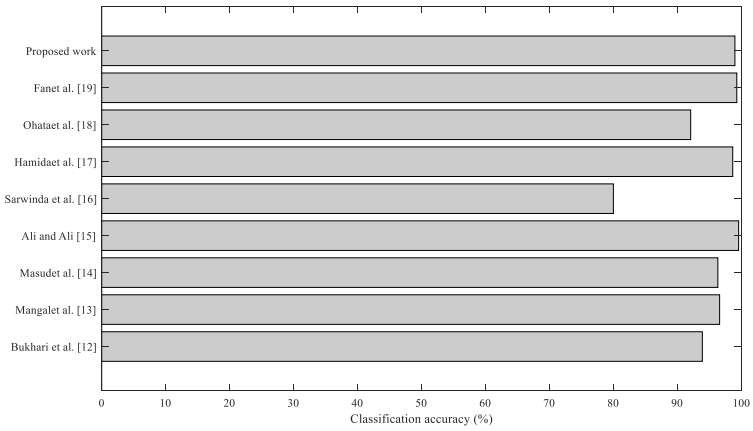

Figure 8. Evaluation of classification accuracy between proposed and existing methods.

This research presented a DLF to detect CC using histological images with individual, fused, and ensemble features. The chief merit of this technique is that it considers the pre-trained deep learning methods, which are pretty simple in their implementation as compared to the customary model. Furthermore, the concept of the fused and ensemble features employed in this technique are also quite simple compared to other similar techniques existing in the literature. Moreover, the result achieved with the LS25000 and GlaS datasets with this DLF confirms its clinical significance.

Figure 8 presents a comparative analysis between the proposed and existing technique. The results of this comparison confirm that this scheme works well. Furthermore, compared to the results displayed in Table 1, the accuracy achieved in the presented work is either improved or closer, confirming that the implemented technique can work well on the clinically collected histology slides. The detection accuracy achieved with the proposed DLF is satisfactory and works well on the chosen database. This research considered the pre-processed GlaS database, and in future, the proposed scheme can be improved to examine the WSI with better accuracy.

5. Conclusions

Early detection of cancer is essential to save the patient with appropriate treatment. This research aims to develop and implement a pre-trained DLF to detect CC in histology slides with an improved accuracy. The proposed scheme considered three classes of deep features, individual, fused, and ensemble, to achieve better detection accuracy using chosen binary classifiers along with a 5-fold cross-validation. The experimental work implemented on LS25000 and GlaS database confirms the merit of the proposed scheme in detecting CC using histology slides. The result achieved with fused deep features confirms that the CC detection accuracy is better than the individual and ensemble features. The proposed scheme achieved a maximum accuracy of 99% when the KNN classifier was employed with fused features. Furthermore, the accuracy achieved with GlaS (benign/malignant classification) was >97% for both the fused and ensemble features. With this result, it can be confirmed that the presented scheme works well on the histology slides. In the future, examining the clinically collected histology slides can be considered.

Use of AI tools declaration

The authors declare they have not used Artificial Intelligence (AI) tools in the creation of this article.

Acknowledgments

This research was partly supported by the Technology Development Program of MSS (No. S3033853) and by the research grant of the Kongju National University in 2023.

Conflict of interest

The authors declare that they have no conflicts of interest to report regarding the present study.

References

1. S. Meyer, W. A. Groenewald, R. D. Pitcher, Diagnostic reference levels in low-and middle-income countries: early “ALARAm” bells?, *Acta Radiol.*, **58** (2017), 442–448. https://doi.org/10.1177/0284185116658681
2. H. Yadav, D. Shah, S. Sayed, S. Horton, L. F. Schroeder, Availability of essential diagnostics in ten low-income and middle-income countries: results from national health facility surveys, *Lancet Global Health*, **9** (2021), e1553–e1560. https://doi.org/10.1016/S2214-109X(21)00442-3

3. J. Naz, M. A. Khan, M. Alhaisoni, S. Kadry, Segmentation and classification of stomach abnormalities using deep learning, *Comput. Mater. Continua*, **69** (2021), 607–625. https://doi.org/10.32604/cmc.2021.017101
4. M. A. Khan, M. S. Sarfraz, M. Alhaisoni, I. Ashraf, StomachNet: Optimal deep learning features fusion for stomach abnormalities classification, *IEEE Access*, **8** (2020), 197969–197981. https://doi.org/10.1109/ACCESS.2020.3034217
5. *World Health Organization*, Cancer, 2022. Available from: https://www.who.int/news-room/fact-sheets/detail/cancer.
6. Colorectal cancer statistics, 2020. Available from: https://www.wcrf.org/cancer-trends/colorectal-cancer-statistics/.
7. M. A. Khan, I. M. Nasir, Y. Nam, A blockchain based framework for stomach abnormalities recognition, *Comput. Mater. Continua*, **67** (2021), 141–158. https://doi.org/10.32604/cmc.2021.013217
8. A. Majid, M. A. Khan, M. Yasmin, U. Tariq, Classification of stomach infections: a paradigm of convolutional neural network along with classical features fusion and selection, *Microsc. Res. Tech.*, **83** (2020), 562–576. https://doi.org/10.1002/jemt.23447
9. Y. Jiao, J. Li, C. Qian, S. Fei, Deep learning-based tumor microenvironment analysis in colon adenocarcinoma histopathological whole-slide images, *Comput. Methods Programs Biomed.*, **204** (2021), 106047. https://doi.org/10.1016/j.cmpb.2021.106047
10. Tissue Image Analytics Centre. Available from: https://warwick.ac.uk/fac/cross_fac/tia/data/glascontest/.
11. K. Sirinukunwattana, J. P. Pluim, H. Chen, A. Böhm, Gland segmentation in colon histology images: the glas challenge contest, *Med. Image Anal.*, **35** (2017), 489–502. https://doi.org/10.1016/j.media.2016.08.008
12. S. U. K. Bukhari, A. Syed, S. K. A. Bokhari, S. S. H. Shah, The histological diagnosis of colonic adenocarcinoma by applying partial self supervised learning, *MedRxiv*, **2** (2020), 1–11. https://doi.org/10.1101/2020.08.15.20175760
13. S. Mangal, A.Chaurasia, A. Khajanchi, Convolution neural networks for diagnosing colon and lung cancer histopathological images, preprint, arXiv: 2009.03878.
14. M. Masud, N.Sikder, A. A.Nahid, M. A. AlZain, A machine learning approach to diagnosing lung and colon cancer using a deep learning-based classification framework, *Sensors*, **21** (2021), 748. https://doi.org/10.3390/s21030748
15. M. Ali, R. Ali, Multi-input dual-stream capsule network for improved lung and colon cancer classification, *Diagnostics*, **11** (2021), 1485. https://doi.org/10.3390/diagnostics11081485
16. D. Sarwinda, R. H. Paradisa, A. Bustamam, P. Anggia, Deep learning in image classification using residual network (ResNet) variants for detection of colorectal cancer, *Proc. Comput. Sci.*, **179** (2021), 423–431. https://doi.org/10.1016/j.procs.2021.01.025
17. A. B. Hamida, M. Devanne, J. Weber, C.Truntzer, C. Wemmert, Deep learning for colon cancer histopathological images analysis, *Comput. Biol. Med.*, **136** (2021), 104730. https://doi.org/10.1016/j.compbiomed.2021.104730

18. E. F. Ohata, J. V. S. D. Chagas, G. M.Bezerra, V. H. C. de Albuquerque, A novel transfer learning approach for the classification of histological images of colorectal cancer, *J. Supercomput.*, **77** (2021), 9494–9519. https://doi.org/10.1007/s11227-020-03575-6
19. J. Fan, J. Lee, Y. Lee, A transfer learning architecture based on a support vector machine for histopathology image classification, *Appl. Sci.*, **11** (2021), 6380. https://doi.org/10.3390/app11146380
20. V. Siripoppohn, R. Pittayanon, K. Tiankanon, N. Faknak, R. Rerknimitr, Real-time semantic segmentation of gastric intestinal metaplasia using a deep learning approach, *Clin Endoscopy*, **55** (2022), 390–400. https://doi.org/10.5946/ce.2022.005
21. V. de Almeida Thomaz, C. A. Sierra-Franco, A. B. Raposo, Training data enhancements for improving colonic polyp detection using deep convolutional neural networks, *Artif. Intell. Med.*, **111** (2021), 101988. https://doi.org/10.1016/j.artmed.2020.101988
22. A. A. Borkowski, M. M. Bui, L. B. Thomas, S. M. Mastorides, Lung and colon cancer histopathological image dataset (lc25000), Preprint, arXiv: 1912.12142.
23. S. Kadry, V. Rajinikanth, D. Taniar, X. P. B. Valencia, Automated segmentation of leukocyte from hematological images—a study using various CNN schemes, *J. Supercomput.*, **78** (2022), 6974–6994. https://doi.org/10.1007/s11227-021-04125-4
24. M. A. Khan, M. Azhar, K. Ibrar, Y. J. Kim, B. Chang, COVID-19 classification from chest X-ray images: a framework of deep explainable artificial intelligence, *Comput. Intell. Neurosci.*, **2022** (2022). https://doi.org/10.1155/2022/4254631
25. S. Kadry, G. Srivastava, V. Rajinikanth, Y. Kim, Tuberculosis detection in chest radiographs using spotted hyena algorithm optimized deep and handcrafted features, *Comput. Intell. Neurosci.*, **2022** (2022). https://doi.org/10.1155/2022/9263379
26. R. Biju, W. Patel, V. Rajinikanth, Framework for classification of chest x-rays into normal/covid-19 using Brownian-mayfly-algorithm selected hybrid features, *Math. Probl. Eng.*, **2022** (2022). https://doi.org/10.1155/2022/6475808
27. F. Afza, M. Sharif, M. A. Khan, J. Cha, Multiclass skin lesion classification using hybrid deep features selection and extreme learning machine, *Sensors*, **22** (2022), 799. https://doi.org/10.3390/s22030799
28. M. Sharif, T. Akram, M. Raza, A. Rehman, Hand-crafted and deep convolutional neural network features fusion and selection strategy: An application to intelligent human action recognition, *Appl. Soft Comput.*, **87** (2020), 105986. https://doi.org/10.1016/j.asoc.2019.105986
29. M. Arshad, U. Tariq, A. Armghan, F. Alenezi, M. Younus Javed, A Computer-aided diagnosis system using deep learning for multiclass skin lesion classification, *Comput. Intell. Neurosci.*, **21** (2021), 1–23. https://doi.org/10.1155/2021/9619079
30. M. Sharif, T. Akram, M. Raza, T. Saba, A. Rehman, Hand-crafted and deep convolutional neural network features fusion and selection strategy: An application to intelligent human action recognition, *Appl. Soft Comput.*, **87** (2020), 105986. https://doi.org/10.1016/j.asoc.2019.105986

AIMS Press